Quaternary Research 83 (2015) 298–306

Contents lists available at ScienceDirect

Quaternary Research

journal homepage: www.elsevier.com/locate/yqres

Seawater temperature seasonality in the South China Sea during the late Holocene derived from high-resolution Sr/Ca ratios of *Tridacna gigas*

Hong Yan [a,b,*], Liguang Sun [b], Da Shao [b], Yuhong Wang [c]

[a] State Key Laboratory of Loess and Quaternary Geology, Institute of Earth Environment, Chinese Academy of Sciences, Xi'an, 710075, China
[b] Institute of Polar Environment, School of Earth and Space Sciences, University of Science and Technology of China, Hefei, Anhui 230026, China
[c] Department of Chemistry and Laser Chemistry Institute, Fudan University, Shanghai 200433, China

ARTICLE INFO

Article history:
Received 7 January 2014
Available online 17 January 2015

Keywords:
South China Sea
Tridacna gigas
Sr/Ca
Temperature seasonality
Late Holocene

ABSTRACT

Temperature seasonality, the difference between summer and winter temperature, has significant influences on global terrestrial and marine ecosystems. However, most of proxy-based climate records are of limited temporal resolution and thus insufficient to quantify the past temperature seasonality. In this study, high-resolution Sr/Ca ratios of modern (live-caught) and fossil (dead-collected) *Tridacna gigas* shells from the South China Sea (SCS) were used to reconstruct the seawater temperature seasonality during the late Holocene. The averaged seawater temperature seasonality around 2165 ± 75 BC (4.46 ± 1.41°C, derived from the data of 18 yr) were similar to the seasonality of recent decade (4.41 ± 0.82°C during AD 1994–2005), but the temperature seasonality around AD 50 ± 40 (3.69 ± 1.37°C, derived from the data of 48 yr) and AD 990 ± 40 (3.64 ± 0.87°C, derived from the data of 11 yr) was significantly lower than that during AD 1994–2005. The reduced seasonality around AD 990 ± 40 was attributable to the unusually warm winter during the medieval times, probably caused by the weakening of East Asian Winter Monsoon. Our study highlighted the potential of *T. gigas* shells in providing high-resolution seasonality climate information during the late Holocene.

Introduction

Changes of temperature seasonality are important components of the climate system: they can have dramatic impacts on ecosystems and human activities (Andreasson and Schmitz, 2000; Smetacek and Nicol, 2005; Patterson et al., 2010; Wanamaker et al., 2011), and assessing past seasonality changes in different climate states is essential for understanding past climatic dynamics and predicting future climate. However, most of current proxy-based climate reconstructions are of annual to decadal resolution and high-resolution paleoclimate records that can quantify temperature seasonality remain scarce.

Many researchers demonstrated that the archives from fast-growing marine biogenic carbonate, such as corals and bivalve shells, are sensitive to surrounding environmental changes, and they could provide high-resolution seasonal/monthly climate records from tropics to high latitudes and have the potential to approach the full seasonal range of past sea-surface temperature (SST) (Cole et al., 1993; Gagan et al., 1994; McCulloch et al., 1994; Schöne et al., 2004a, 2004b; Watanabe et al., 2004; Schöne et al., 2005a; Wanamaker et al., 2008; Aubert et al., 2009; Elliot et al., 2009; Maier and Titschack, 2010; Batenburg et al., 2011; Yan et al., 2011a). For example, a number of climatic seasonality reconstructions based on bivalve sclerochronology and bivalve proxies have been reported in recent decades (Jones and Allmon, 1995; Andreasson and Schmitz, 1996; Bojar et al., 2004; Schöne et al., 2005b; Goewert and Surge, 2008; Schöne and Fiebig, 2009; Patterson et al., 2010; Wanamaker et al., 2011; Surge and Barrett, 2012; Wang et al., 2012, 2013). These high-resolution seasonal/monthly archives greatly help us in reconstructing the regional climate history and understanding the past climate dynamics.

The marine bivalve, *Tridacna* spp., is a prominent member of the Indo-Pacific coral reef communities from Eocene to present (Rosewater, 1965). *Tridacna gigas* is the largest bivalve species, it can grow to over 1 m in length and live up to 100 yr (Rosewater, 1965), and it has hard and dense aragonite shells with daily growth lines in their inner shell layer, an ideal material for high-resolution paleoclimate reconstructions (Aharon and Chappell, 1986; Watanabe and Oba, 1999). The oxygen isotope ratios ($\delta^{18}O$) of *Tridacna* specimens, which calcifies essentially in isotopic equilibrium with surrounding seawater, have been mainly used as the evidence for late Quaternary temperature changes (Aharon et al., 1980; Aharon, 1983; Aharon and Chappell, 1986; Aharon, 1991; Watanabe et al., 2004; Yan et al., 2014c). However, $\delta^{18}O$ of marine biogenic carbonate is influenced by both SST and seawater $\delta^{18}O$, and the interpretation of $\delta^{18}O$ as a proxy for SST

* Corresponding author at: State Key Laboratory of Loess and Quaternary Geology, Institute of Earth Environment, Chinese Academy of Sciences, Xi'an, 710075, China.
E-mail address: yanhong@ieecas.cn (H. Yan).

http://dx.doi.org/10.1016/j.yqres.2014.12.001
0033-5894/

has large uncertainties, especially in areas with large salinity variations (Cole et al., 1993; McCulloch et al., 1994).

The Sr/Ca ratio, which has been extensively utilized as paleothermometers in corals (Beck et al., 1992; McCulloch et al., 1994, 1996; Alibert and McCulloch, 1997), has also been investigated recently in *Tridacna* specimens (Elliot et al., 2009; Batenburg et al., 2011; Sano et al., 2012; Yan et al., 2013, 2014a). In our previous study, the high-resolution Sr/Ca ratios of modern *T. gigas* specimen from the South China Sea were determined by ICP-OES; the Sr/Ca profiles had clear annual cycles, they were significantly correlated with the local SST, and they could be used as SST proxies (Yan et al., 2013). Meanwhile, the within-species differences were insignificant and the Sr/Ca ratios of different modern specimens in the same species seemed to have good reproducibility (Yan et al., 2014a). These studies highlighted the potentials of using the Sr/Ca profiles of *Tridacna* specimens to reconstruct the high-resolution paleo-temperature.

In addition to modern specimens (Yan et al., 2013, 2014a), we have also analyzed the Sr/Ca ratios of two fossil *T. gigas* shells, dated around AD 50 ± 40 and AD 990 ± 40, respectively, and reconstructed the SST variations in the South China Sea during the late Holocene natural warm periods of Medieval Climate Anomaly (MCA, ≈AD 800–1300) and Roman Warm Period (RWP, ≈200 BC–AD 400) (Yan et al., 2014b).

The South China Sea is the largest marginal sea of the western tropical Pacific, and its climate variations are influenced by both the East Asian Monsoon and the tropical Pacific ENSO conditions. Thus the high-resolution seasonal climate archives from the South China Sea are important for investigating the interactions between tropics and the Northern Hemisphere high latitudes. Based upon the published high-resolution *T. gigas* Sr/Ca profiles, together with the new Sr/Ca data of another fossil *T. gigas* specimen dated around 2165 ± 75 BC, in the present study we examine the changes of seawater temperature seasonality in the South China Sea and discuss the interactions between high and low latitudes during the late Holocene.

Materials and methods

Regional settings

The South China Sea (SCS) is located in the far western tropical Pacific; it is a semi-enclosed marginal sea with an area of ~3.6 million km^2 (Fig. 1). SCS consists of hundreds of islands, including Nansha Islands (Spratly Islands), Xisha Islands (Paracel Islands), Zhongsha Islands (Macclesfield Islands), and Dongsha Islands (Pratas Islands). Yongxing Island (16°50′N, 112°20′E), Shidao Island (16°50′, 112°20′) and Dongdao Island (16°40′N, 112°44′E) are located in the Xisha Islands, and they are elliptical tropic reef islands with a land area of 2.13 km^2, 0.08 km^2 and 1.55 km^2, respectively (Yan et al., 2010b).

Meteorological observations (air temperature, precipitation) in Yongxing Island have been made since 1958 by the Institute of Meteorology of China. The SST data in Xisha Islands were obtained from NOAA NCEP EMC CMB GLOBAL Reyn_SmithOIv2 data (a global weekly SST data from 1982 with a spatial resolution of 1° × 1°), where the grid cell of the NOAA data was selected to include Yongxing Island. Figure 2 shows monthly-averaged time series of air temperature, rainfall and SST from 1982 to 2005. The average annual rainfall (AD 1982–2005) of Xisha Islands is about 1443 mm. The dry and wet seasons are very clear. 82% of total precipitation occurs from June to November due to the effect of southwest monsoon. The average annual AT and SST (AD 1982–2005) are 26.94 and 27.59°C, respectively (Yan et al., 2010a, 2011b).

Shell collection and sample preparation

Four *T. gigas* specimens from the Xisha Islands were used in this study (Figs. 1 and 3). One specimen of *T. gigas*, named YX1, was collected alive from the broad coral reef in the north of Yongxing Island, South China Sea, on March 2005 (Yan et al., 2013). YX1 is 14 cm high and 19 cm long (Yan et al., 2013). The *T. gigas* specimens SD1, DD1 and DD2 were discovered dead on the beach of Shidao Island and in the interior area of Dongdao Island, respectively (Yan et al., 2014b). The SD1 was 32 cm

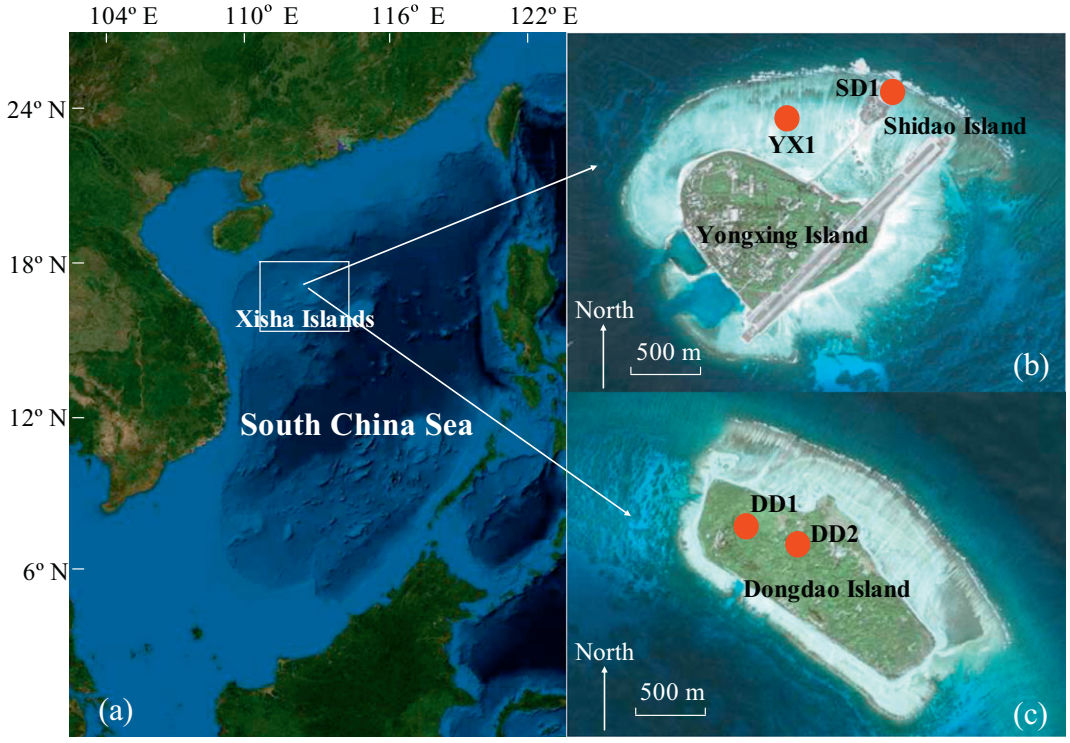

Figure 1. Left: map of SCS. Right: map of Yongxing Island, Shidao Island and Dongdao Island in Xisha archipelago. The sampling sites of *Tridacna gigas* specimens are marked by red dots.

https://doi.org/10.1016/j.yqres.2014.12.001 Published online by Cambridge University Press

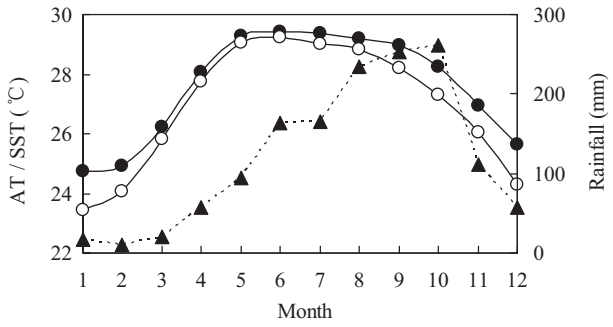

Figure 2. Monthly mean air temperature (AT, hollow dots), rainfall (triangles) and SST (SST, solid dots) in Yongxing Island from 1982 to 2008.

high and 51 cm long, the DD1 was 44 cm high and 52 cm long, and the DD2 was 39 cm high and 76 cm long (Yan et al., 2014b).

X-ray diffraction (XRD) analysis suggested that the *T. gigas* shells studied here were entirely made of aragonite, consistent with previous studies on *T. gigas* specimens (Watanabe et al., 2004; Yan et al., 2013, 2014b). The collected shells were first ultrasonically rinsed with de-ionized water and then air-dried. A 5 mm thick ontogenetic record was obtained by sampling a radial section of each *T. gigas* shells along a plane passing from the oldest past (umbo) to the growing margin that represented the axis of maximum growth (Fig. 3a) (Watanabe et al., 2004; Yan et al., 2013, 2014b).

Sr/Ca analysis and AMS ^{14}C dating

Powder samples for Sr/Ca analysis were obtained along the sampling lines, which were perpendicular to the annual bands of each *T. gigas* specimens, using a micro drill (Yan et al., 2013, 2014b). The Sr/Ca data of YX1, SD1 and the first 15 yr of DD1 were reported in our previous study (Yan et al., 2013, 2014b). In this study, we sampled DD2 and the additional 33 annual bands of DD1 with the intervals of 0.2 mm. Please see the previous studies for the detailed method for Sr/Ca analysis of subsamples (Yan et al., 2013, 2014b). Raw elemental concentration data (Ca and Sr) were drift-corrected using the sample-standard correction method (Schrag, 1999). External precision of a laboratory standard was ±0.46% for Sr/Ca (2.183 ± 0.001 mmol/mol).

One powder sample of SD1, one powder sample for DD2 and two powder samples of DD1 were taken in the middle of the sections of the SD1, DD1 and DD2 for AMS ^{14}C measurements (Yan et al., 2014b). The analyses were performed at the Institute of Earth Environment of CAS and the Earth System Science Department, University of California, Irvine, California, USA.

Data resampling

In order to assess SST seasonality from Sr/Ca profiles, we resampled data within each year with a 10-point cubic spline model (Schöne and Fiebig, 2009; Wanamaker et al., 2011) using AnalySeries (version 2.0.4.2, freely available at http://www.lsce.ipsl.fr/en/softwares/index.php). The resampling (10 samples/yr for all four shells) minimizes potential biases related to variability in growth rate (Wanamaker et al., 2011).

Calculating SST using T. gigas Sr/Ca ratios

Two calibration equations between Sr/Ca ratios of modern *T. gigas* specimen and instrumental SST, based on all monthly data and extremum data (January, June and July), were established in our previous work (Yan et al., 2013). The regression based on all monthly data yielded the following equation: SST (°C) = 60.10 − 14.41 × Sr/Ca (mmol/mol), $r^2 = 0.71$, n = 133, while the regression based on extremum data (January, June and July data) yielded the equation: SST (°C) = 64.93 − 16.60 × Sr/Ca (mmol/mol), $r^2 = 0.95$, n = 34. The standard deviation of the residuals of the regressions suggested that the equation from monthly data had larger uncertainty due to the errors in age model, and the equation

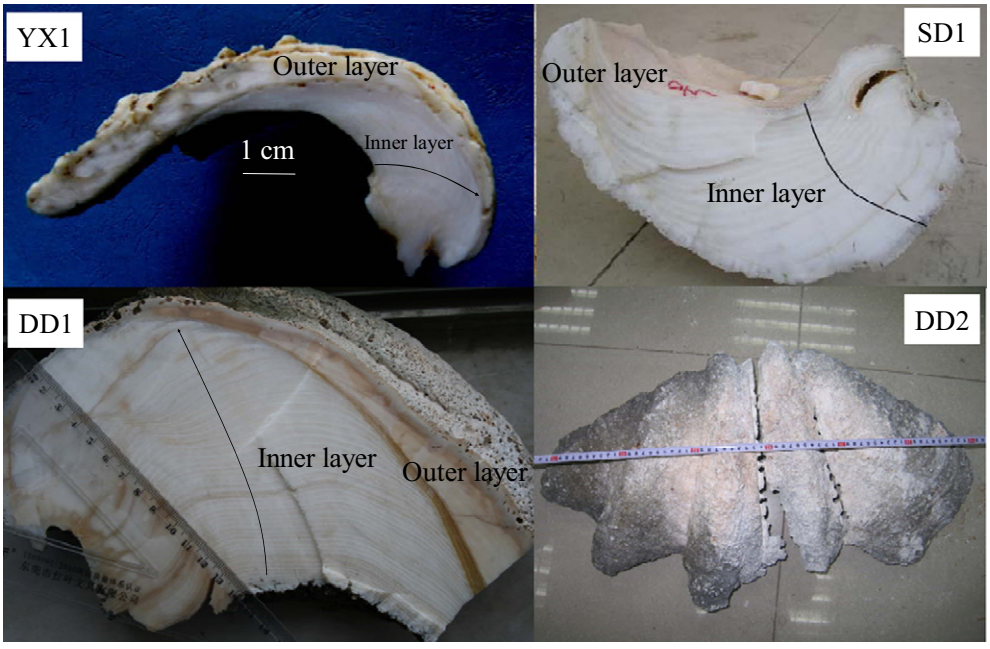

Figure 3. The radial sections of *T. gigas* specimens YX1, SD1, DD1 and DD2 in this study. The radial section reveals two distinct growth zones: the inner shell and the outer shell layer. Black lines indicate the sampling lines for Sr/Ca ratios.

https://doi.org/10.1016/j.yqres.2014.12.001 Published online by Cambridge University Press

from extremum data produced better SST prediction (see Yan et al., 2013 for details). Therefore, here we used the equation from the extremum data to calculate the SST during the late Holocene warm periods.

Results

Sr/Ca ratios of YX1, SD1, DD1 and DD2 determined by ICP-OES

Seasonal oscillations are evident in the Sr/Ca ratio profiles of YX1, SD1, DD1 and DD2 determined by ICP-OES (Fig. 4). About 11, 11, 48 and 18 annual cycles are detected in Sr/Ca profiles of YX1, SD1 DD1 and DD2, respectively. Average Sr/Ca ratios of YX1, SD1, DD1 and DD2 are 2.24 ± 0.10 mmol/mol (n = 188), 2.18 ± 0.10 mmol/mol (n = 198), 2.12 ± 0.10 mmol/mol (n = 725) and 2.32 ± 0.12 mmol/mol (n = 209), ranging from 2.04 to 2.44 mmol/mol, 1.93 to 2.39 mmol/mol, 1.88 to 2.51 mmol/mol and 1.96 to 2.63 mmol/mol, respectively (Fig. 4).

The Sr/Ca ratios of studied *Tridacna* specimens in this study (ranging from 1.88 to 2.63 mmol/mol) are comparable to those of *Tridacna* Sr/Ca ratios from Indonesia (1.44–2.84 mmol/mol, *Tridacna sqamosa*)(Batenburg et al., 2011), Papua New Guinea(1.4–1.9 mmol/mol, *T. gigas*) (Elliot et al., 2009), Australia (1.4–1.8 mmol/mol, *T. gigas*) (Elliot et al., 2009) and Ishigaki Island (1.2–2.0 mmol/mol, *Tridacna derasa*) (Sano et al., 2012), but much lower than typical coral Sr/Ca ratios (from 7.5 to 9.5 mmol/mol) (Wei et al., 2000; Yu et al., 2005a,b; Corrège, 2006; Wei et al., 2007). It implies that the partition coefficients D_{Sr} ($D_{Sr} = [Sr/Ca]_{shell}/[Sr/Ca]_{water}$) are significantly different between coral and bivalve aragonite.

Series of shells

The *T. gigas* specimen YX1 was live-collected in March 2005, so the 11 cycles in Sr/Ca profile of YX1 corresponded to 11 yearly growth patterns from 1994 to 2005 (Fig. 4) (Yan et al., 2013). The AMS dating results of SD, DD1 and DD2 were 1460 ± 15 ^{14}C yr BP (SD1), 2340 ± 15 ^{14}C yr BP (DD1), 2305 ± 15 ^{14}C yr BP (DD1) and 3756 ± 37 ^{14}C yr BP (DD2), respectively (Table 1). The two dating results of the specimen DD1 were close to each other, implying that the AMS ^{14}C dating method has a good reproducibility for *Tridacna* samples. The conventional radiocarbon ages were corrected to 960 ± 40 cal yr BP (AD 990 ± 40), 1920 ± 40 cal yr BP (AD 30 ± 40), 1880 ± 40 cal yr BP (AD 70 ± 40) and 4115 ± 75 cal yr BP (2165 ± 75 BC) using CalPal-2007-marine (Hughen et al., 2004; Weninger et al., 2007). The Sr/Ca ratios of SD1, DD1 and DD2, therefore, had the potential to record the climate information around AD 990 (±40), AD 50 (±40) and 2165 (±75) BC, respectively.

Detailed chronologies for high-resolution Sr/Ca profiles of YX1, SD1, DD1 and DD2 were established using the annual arrival-times of the winter SST minima at Yongxin Island. The time for the data point of

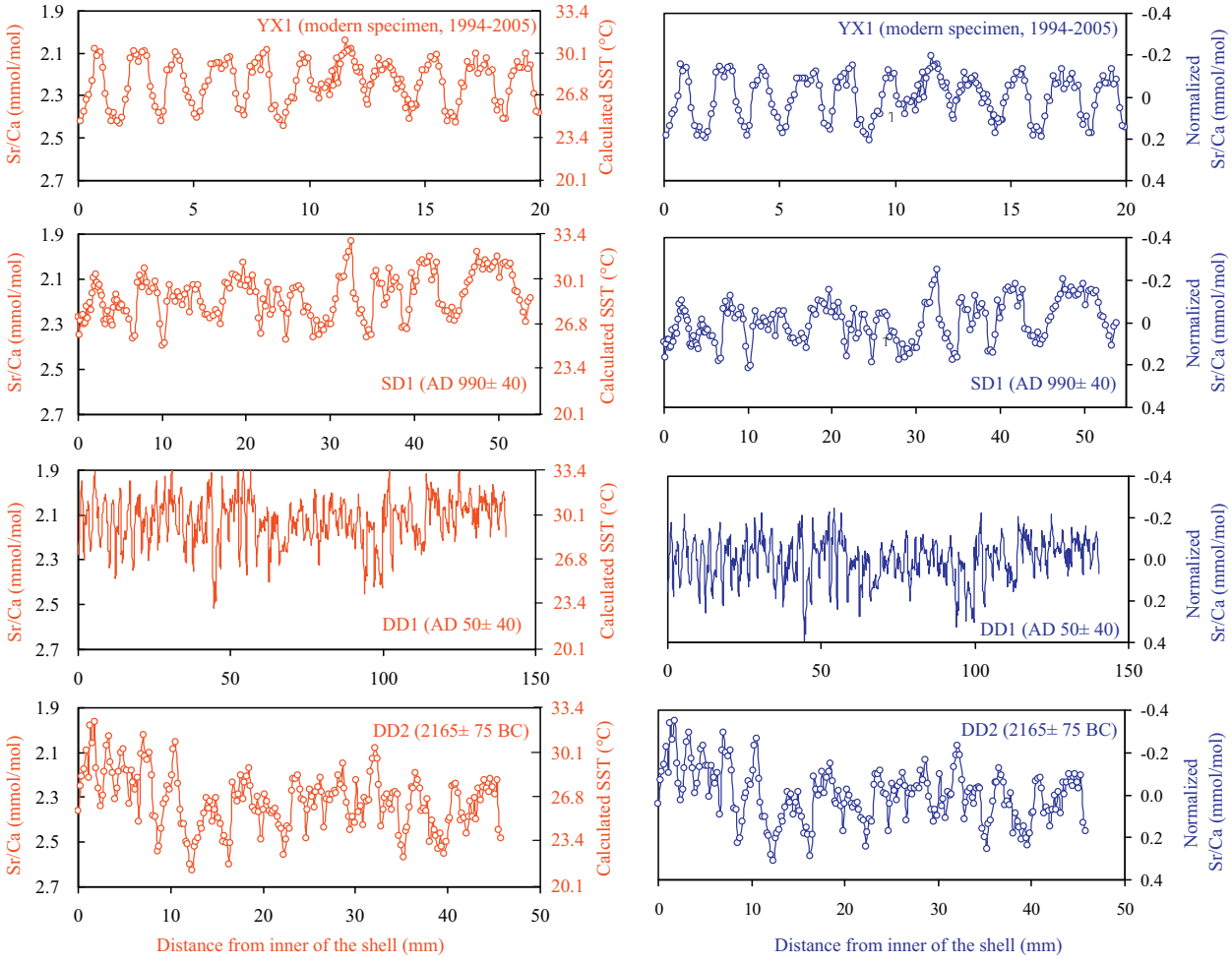

Figure 4. Left: Sr/Ca profiles of *T. gigas* specimens YX1, SD1, DD1 and DD2. The abscissa is the distance between the sampling site and the inner surface of the shell. Right: the normalized Sr/Ca profiles prior to resampling for each of the four shells in this study.

https://doi.org/10.1016/j.yqres.2014.12.001 Published online by Cambridge University Press

Table 1
AMS ^{14}C dating results.

Sample number	Material	^{14}C conventional age (yr BP)	Calibrated age (cal yr BP) 2 sigma	Calibrated age (BC/AD) 2 sigma
sdcq-4 (SD-1)	Carbonate powder	1460 ± 15	960 ± 40	AD 990 ± 40
ddcq-3 (DD-1)	Carbonate powder	2340 ± 15	1920 ± 40	AD 30 ± 40
ddcq-2 (DD-1)	Carbonate powder	2305 ± 15	1880 ± 40	AD 70 ± 40
dd-2 (DD-2)	Carbonate powder	3756 ± 37	4115 ± 75	2165 ± 75 BC

maximum Sr/Ca was assigned January, and the time for the data points between the Sr/Ca maxima was assigned using linear interpolation with equal time span (Yan et al., 2013, 2014b).

Data resampling and calculation of seawater temperature seasonality

Relatively high-resolution Sr/Ca data of the four shells (averaged 16 samples per year and at least 10 samples per year) allow for a minimum of 10 samples per year to be obtained from each annual growth increment (Wanamaker et al., 2011). The resampling results of four shells using AnalySeries 2.0.4.2 (cubic spline model) are shown in Figure 5. Before resampling, the Sr/Ca data were normalized by subtracting the mean Sr/Ca value (Fig. 4).

The shapes of resampled Sr/Ca profiles show an obvious wide summer portion and a narrow winter portion of each annual cycle (Fig. 5), similar to the shape of monthly SST variation (Fig. 2). In this study, instrumental SST seasonality is defined as the difference between summer (average of June, July and August) and winter (average of January and February) SSTs, and proxy SST seasonality is defined as the difference between SSTs reconstructed from summer and winter Sr/Ca values (Δ Sr/Ca). For resampled Sr/Ca ratios of each year, the greatest Sr/Ca ratio is used as the winter Sr/Ca value, while the average of two smallest Sr/Ca ratios is used as the summer Sr/Ca value. Using the *T. gigas* Sr/Ca-SST equation derived from YX1 in previous study (Yan et al., 2013),

$$\mathrm{SST}(^{\circ}\mathrm{C}) = 64.93 - 16.60 \times \mathrm{Sr/Ca(mmol/mol)}. \quad (1)$$

Proxy SST seasonality can be calculated using following equation:

$$\text{Proxy SST seasonality } \mathrm{T}(^{\circ}\mathrm{C}) = 16.60 \times \Delta\mathrm{Sr/Ca}. \quad (2)$$

Based upon Eq. (2), we calculated proxy seasonality from 1994 to 2005 using the data from YX1. The modern instrument SST seasonality from 1994 to 2005 in this region is 4.31 ± 0.69°C. The proxy SST seasonality derived from ΔSr/Ca of YX1 is 4.41 ± 0.82°C, and it is significantly correlated with the instrumental SST seasonality (Fig. 6c, $r = 0.63$, $p < 0.05$, $n = 11$). The noticeable scattering of the estimated seasonality away from the 1:1 line is likely caused by reasons such as the errors in *T. gigas* Sr/Ca-SST calibration, the errors in the age models of Sr/Ca series and the mismatch between calculated seasonality and real seasonality.

Calibrated proxy SST seasonality for the last 2000 yr

The calibrated proxy SST seasonality of modern and fossil *T. gigas* specimens are plotted in Figure 7, and for convenience of discussion it will be called SST seasonality hereinafter. The modern (live-caught) shell (YX1) had a mean SST seasonality of 4.41 ± 0.82°C (mean winter Sr/Ca value = 2.39 ± 0.04 mmol/mol; mean summer Sr/Ca value = 2.12 ± 0.02 mmol/mol; mean ΔSr/Ca = 0.27 ± 0.05 mmol/mol) from AD 1994 to 2005 (Fig. 7). The fossil shell SD1, living in the early MCA based on AMS ^{14}C result (around AD 990 ± 40), had a mean SST seasonality of 3.64 ± 0.87°C (Sr/Ca mean max = 2.31 ± 0.04 mmol/mol; Sr/Ca mean min = 2.10 ± 0.06 mmol/mol; mean ΔSr/Ca = 0.21 ± 0.05 mmol/mol) (Fig. 7). The fossil shell DD1, living in the RWP based on AMS ^{14}C (around AD 50 ± 40), had a mean SST seasonality of 3.69 ± 1.37°C (Sr/Ca mean max = 2.25 ± 0.05 mmol/mol; Sr/Ca mean min = 2.03 ± 0.04 mmol/mol; mean ΔSr/Ca = 0.22 ± 0.05 mmol/mol) (Fig. 7). The fossil shell DD2, living around 2165 ± 75 BC, had a mean SST seasonality of 4.46 ± 1.41°C (Sr/Ca mean max = 2.46 ± 0.09 mmol/mol; Sr/Ca mean min = 2.19 ± 0.09 mmol/mol; mean ΔSr/Ca = 0.27 ± 0.08 mmol/mol) (Fig. 7).

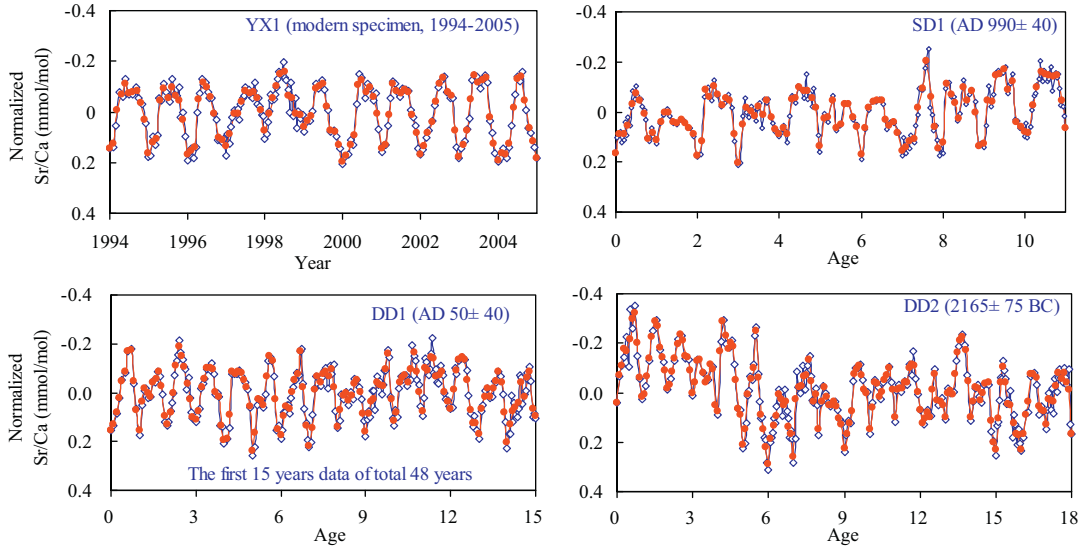

Figure 5. The 10-point resampling using AnalySeries 2.0.4.2 (cubic spline model) for all four shells. The normalized data are shown in blue and the resampled data are shown in red.

https://doi.org/10.1016/j.yqres.2014.12.001 Published online by Cambridge University Press

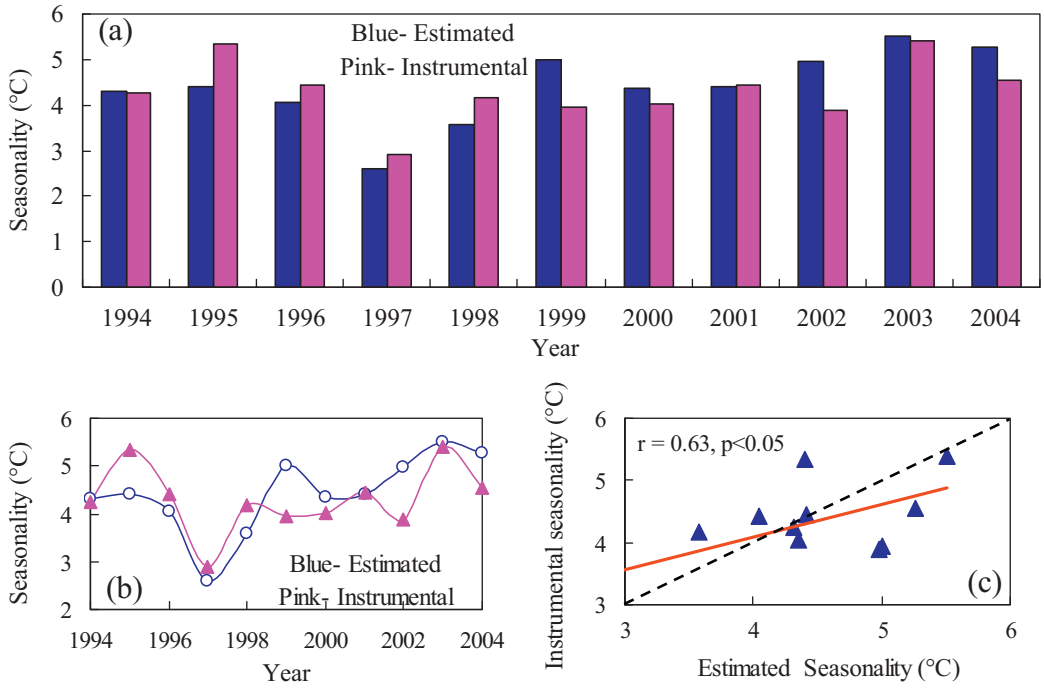

Figure 6. (a and b) The instrumental seasonality (pink) during the 1994–2005 and the estimated seasonality (blue) based on Sr/Ca data of YX1. (c) The linear regression (solid line) and the 1:1 line (dotted line) between the instrumental seasonality and the estimated seasonality.

Discussion

Profiles of seawater temperature variation during the Late Holocene

The mean calibrated proxy SST seasonality of four *T. gigas* shells YX1, SD1, DD1 and DD2 were 4.41 ± 0.82°C, 3.64 ± 0.87°C, 3.69 ± 1.37°C and 4.46 ± 1.41°C, respectively (Fig. 7). The SST seasonality of early MCA shell SD1 (3.64°C) and RWP shell DD1 (3.69°C) were smaller than that of modern *T. gigas* specimen YX1 (4.41°C), while the SST seasonality of shell DD2 around 2165 ± 75 BC (4.46°C) was similar to that of modern specimen. We performed unpaired two-sample *t*-test (unequal sample sizes and equal variance) and examined the differences

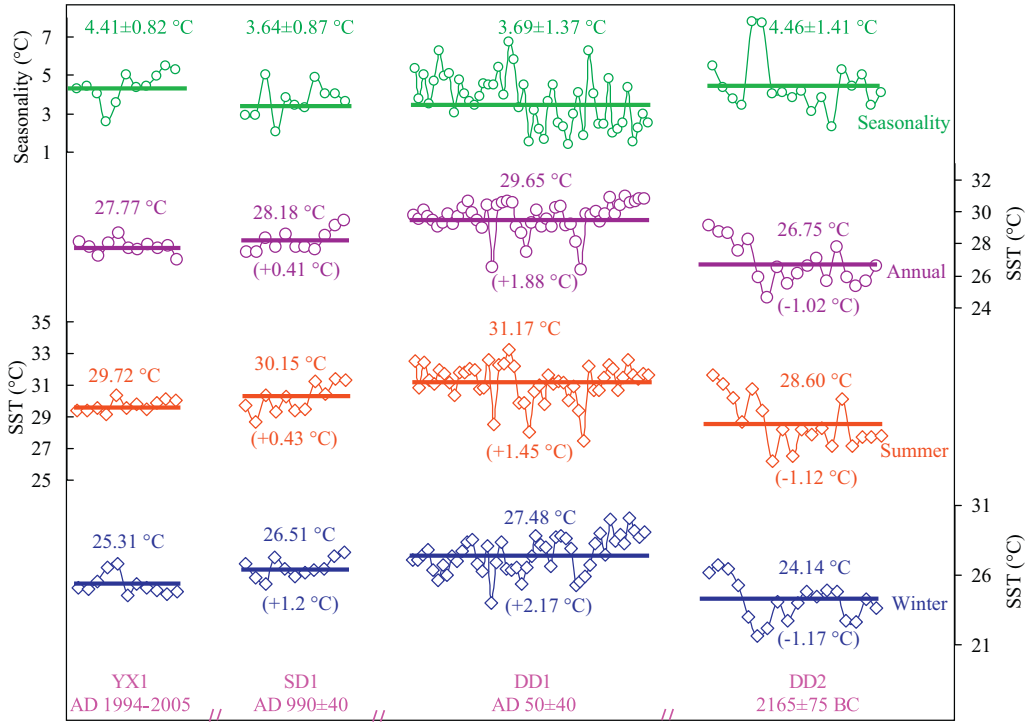

Figure 7. Estimates of seawater temperature seasonality (top, green) for intervals of the late Holocene. The reconstructed annual (purple), summer (red) and winter (blue) SST were plotted.

https://doi.org/10.1016/j.yqres.2014.12.001 Published online by Cambridge University Press

of SST seasonality between modern and each fossil *T. gigas* shell. The SST seasonality difference between DD2 and YX1 was insignificant (YX1 vs. DD2, two-tailed test $P = 0.28$), but the SST seasonality differences between shell SD1, DD1 and YX1 were significant (YX1 vs SD1, two-tailed test $p < 0.05$; YX1 vs DD1, two-tailed test $p < 0.05$).

In order to examine the SST seasonality variations, the calculated annual mean SST, winter and summer SST of four *T. gigas* at four time windows were plotted in Figure 7. The annual mean SSTs were calculated from all resampled Sr/Ca data of each year using Eq. (1). The winter and summer SSTs were derived from the winter and summer Sr/Ca values of each year, respectively.

The annual mean SST around AD 990 ± 40 (SD1) and AD 50 ± 40 (DD1) were 28.18 ± 0.41°C and 29.65 ± 0.99°C, 0.41°C and 1.88°C higher than that during the 1994–2005 (27.77 ± 0.4°C), while the SST seasonality around AD 990 ± 40 (3.64°C) and AD 50 ± 40 (3.69°C) was 0.77°C and 0.72°C smaller than that of recent decade (4.41°C), respectively. The reduced SST seasonality in warmer climate intervals is consistent with the previous bivalve study in Gulf of Maine, which reported increased seasonality with climate cooling (Wanamaker et al., 2011). However, some studies from other areas revealed opposite relations (Surge and Barrett, 2012; Wang et al., 2012). For example, high-resolution $\delta^{18}O$ series of *patella vulgate* shells from Scotland indicated that the warmer early MCA corresponded to larger temperature seasonality (Surge and Barrett, 2012). Meanwhile, we also did not observe any significant difference of seasonality between cold time interval around 2165 ± 75 BC (annual mean SST was 26.75 ± 1.33°C and seasonality was 4.46°C) and the recent decade (annual mean SST was 27.77 ± 0.43°C and seasonality was 4.41°C), pointing to a diverse relationship between the mean SST and the temperature seasonality in northern SCS during the late Holocene (Fig. 7).

The changes of SST seasonality in SCS during the late Holocene could be related with the asynchronous variations of winter and summer SSTs. For the time period of 2165 ± 75 BC, its winter SST difference to that of the recent decade is 1.17°C, comparable to the summer SST difference of 1.12°C. However, for the time windows around AD 990 ± 40 and AD 50 ± 40, their winter SST differences to that of the recent decade are 1.20°C and 2.17°C, respectively, significantly higher than the summer SST differences of 0.43°C and 1.45°C (Fig. 7). This explains why the SST seasonality of the time windows around AD 990 ± 40 and AD 50 ± 40 are significantly smaller than those of other two time windows.

Potential mechanisms for changes in seawater temperature seasonality

SCS lies on the border of East Asia and tropical western Pacific. The climate variation in the SCS is affected by both the East Asian Monsoon and the tropical climate conditions (Yan et al., 2010a, 2011b). The climate records from the SCS are thus important in investigating the couplings and interactions between the tropical climate and the Northern Hemisphere mid-high latitudes.

In order to assess the mechanisms for SST seasonality changes in the SCS during the late Holocene, we first examined the high-resolution instrumental SST data and the results suggested that the summer and winter SSTs in Xisha Islands were probably controlled by different climatic dynamics (Fig. 8). During the summer, the West Pacific Warm Pool (WPWP) migrates northward and the Xisha area is included in the WPWP (Fig. 8). Therefore, the summer temperature in Xisha area may be dominated by the thermodynamic characteristics of WPWP, and the perturbations of WPWP could contribute to the summer temperature anomaly in the region of Xisha Islands. During the winter, the WPWP migrates south away from the Xisha Islands and an interesting "cold tongue" lies in the northern SCS (Fig. 8). The formation of "cold tongue" in northern SCS is likely attributed to the strong East Asian Winter Monsoon. The strong northeast wind brings cold water southward and cools the northern SCS (An et al., 1991). Within the same latitude, the winter SST in Xisha Islands could be 3–5°C colder than that in the east of Philippines (Fig. 8).

Therefore, one would expect that changes of the winter monsoon could have major impacts on the winter SST in Xisha Islands, with stronger winter monsoon corresponding to cooler winter temperature. We analyzed the instrumental data from 1960 to 2000 in northern SCS, examined the potential winter monsoon–temperature connection, and observed a significant negative correlation between 3-year smoothing winter monsoon strength and winter temperature in northern SCS (Fig. 9).

Overall, the summer and winter SSTs in northern SCS are controlled by different climatic dynamics. The summer SST is dominated by WPWP condition, while the winter SST is deeply affected by the East Asian Winter Monsoon. Although the mean SST during the time window around 2165 ± 75 BC (26.75 ± 1.33°C) was remarkably colder than that of the recent decade (27.77 ± 0.43°C), their SST seasonality were similar. The co-variation of summer and winter SST during this time interval was likely caused by the synchronous changes of the East Asian Winter Monsoon and the WPWP condition. In contrast, the asynchronous winter and summer temperature variations during the time windows around AD 990 ± 40 and AD 50 ± 40 pointed to the possible decoupling of East Asian Winter Monsoon and Pacific climate condition during the early MCA and RWP.

The slightly warmer summer SST during MCA than the recent decade (by 0.43°C) indicated a similar WPWP condition, while the significantly warmer winter SST during MCA than the recent decade (by 1.2°C) suggested a significant weaker EAWM around the AD 990 ± 40. Due to lack of high-resolution climate records from the SCS in these time intervals, comparison with other proxy reconstructions

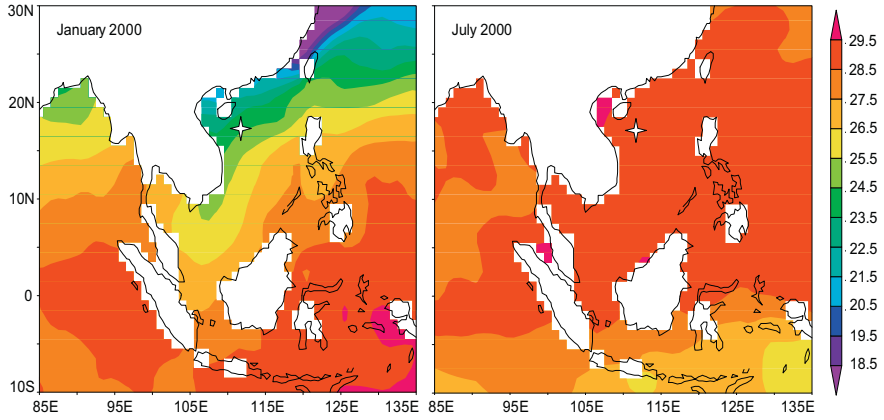

Figure 8. The January and July sea-surface temperature in the South China Sea. The study site Xisha Islands is marked as a star on the maps.

https://doi.org/10.1016/j.yqres.2014.12.001 Published online by Cambridge University Press

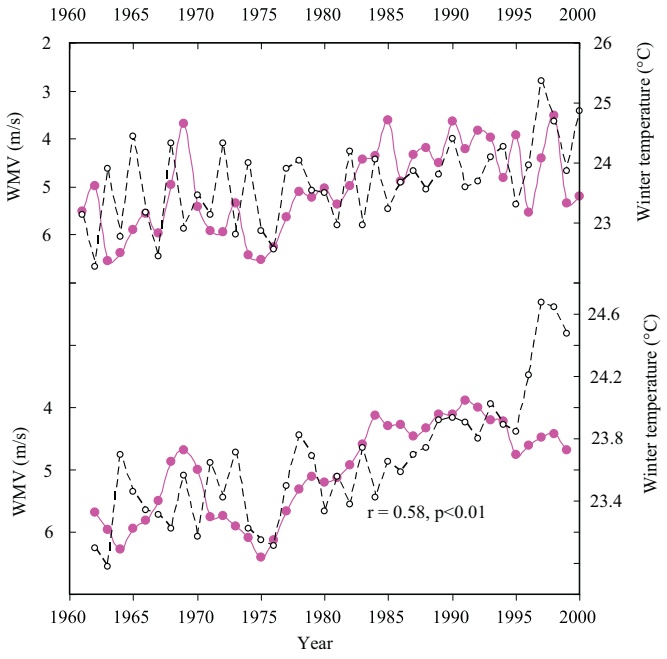

Figure 9. Top: the East Asian Winter Monsoon strength (pink) and winter temperature (black) in Xisha Island from 1961 to 2000. Bottom: the 3-year smoothing East Asian Winter Monsoon strength (pink) and winter temperature (black) in Xisha Island. The winter monsoon velocity (WMV) was used as the East Asian Winter Monsoon strength. The WMV data (December-January-February) were obtained from the observation station in the Yongxing Island and from the meteorological data network (http://www.tutiempo.net/en). The average temperature of December, January and February was used as the winter temperature.

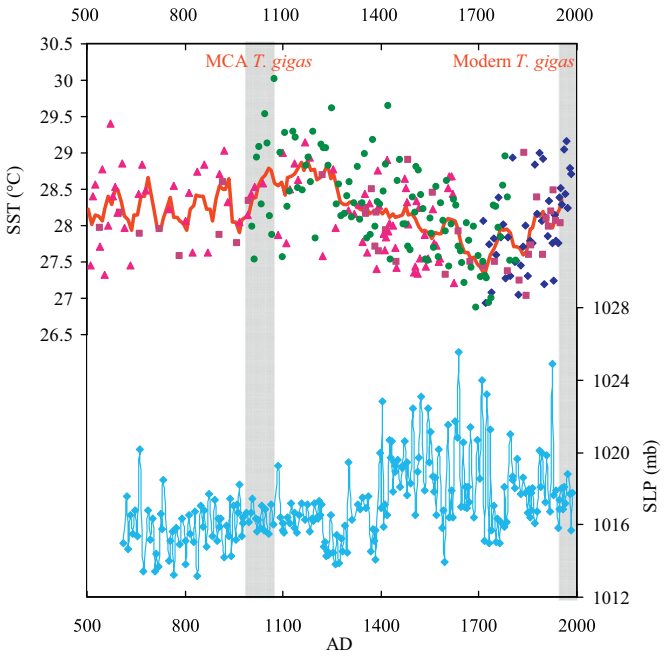

Figure 10. Top: Sea-surface temperature reconstruction in Makassar Strait of Indonesia during the late Holocene derived from the Mg/Ca of planktonic foraminifera in four sediment cores (Oppo et al., 2009). The blue, green, pink and purple points are the reconstructed SST data of the four sediment cores and the red line is their 3-point running mean. The gray bars indicate the times that SD1 and YX1 lived. Bottom: Reconstructed Siberian High sea level pressure (SLP) proxy series based on 3-year resampled GISP 2 log (nssK) series (Meeker and Mayewski, 2002). The Siberian High is strongly coupled with the East Asian Winter Monsoon and is used as a winter monsoon proxy.

is hindered. However, the climate reconstructions from the tropical Pacific and Northern Hemisphere mid-high latitudes could provide some perspectives for the changes of seasonality during the early MCA (Fig. 10) (Meeker and Mayewski, 2002; Oppo et al., 2009). For example, the reconstructed Siberian High index (Fig. 10), one of EAWM proxy, was lower during the early MCA than the recent decades (Meeker and Mayewski, 2002). In other words, the EAWM was weaker in early MCA than in recent decades, and this is consistent with our results of a significantly warmer winter SST in the time interval AD 990 ± 40 than in the recent decade. Meanwhile, the SST records from the Indonesia (Fig. 10), the core area of WPWP, suggested a similar warm pool SST during the early MCA and in the recent decade, also supporting our results of a slightly warmer summer SST around AD 990 ± 40 (Oppo et al., 2009).

Conclusion

In this study, high-resolution Sr/Ca ratios of modern (live-caught) and fossil (dead-collected) *T. gigas* shells from the South China Sea were used to reconstruct the seasonal changes in seawater temperature during the late Holocene. On average, the seawater temperature seasonality around 2165 ± 75 BC (4.46 ± 1.41, 18 yr) is similar to that of the recent decade (4.41 ± 0.82 during AD 1994–2005), but the seawater temperature seasonality around AD 990 ± 40 (3.64 ± 0.87, 11 yr) and AD 50 ± 40 (3.69 ± 1.37, 48 yr) are significantly lower than that of the recent decade. The similar seasonality and synchronous variations of summer and winter SST around 2165 ± 75 BC and AD 1994–2005 are likely caused by the synchronous changes of the East Asian Winter Monsoon and the WPWP condition. In contrast, the reduced seasonality and asynchronous variations of winter and summer SST around AD 990 ± 40 and AD 50 ± 40 pointed to the possible decoupling of East Asian Winter Monsoon and WPWP condition. Early MCA had comparable summer SST with the recent decade and thus a similar WPWP condition, while it had much warmer winter SST than the recent decade, likely attributed to a significantly weaker EAWM. Our study highlighted the potentials of *T. gigas* shells in providing high-resolution seasonality climate information spanning the Holocene or even more. Such information is important for understanding climate dynamics and vital for verifying numerical climate models.

Acknowledgment

Financial support for this research was provided by the Natural Science Foundation of China (NSFC) (41403018, 41176042), Major State Basic Research Development Program of China (973 Program) (2013CB955900), the West Light Foundation of The Chinese Academy of Sciences (29Y42909101) and the Key Programs of the Chinese Academy of Sciences (55ZZBS1304101). We wish to thank Bai Zhou and Shaolong Zhang for their help in sampling and analyzing.

References

Aharon, P., 1983. 140,000-yr isotope climatic record from raised coral reefs in New Guinea. Nature 304, 720–723.
Aharon, P., 1991. Recorders of reef environment histories—stable isotopes in corals, giant clams, and calcareous algae. Coral Reefs 10, 71–90.
Aharon, P., Chappell, J., 1986. Oxygen isotopes, sea level changes and the temperature history of a coral reef environment in New Guinea over the last 105 years. Palaeogeography, Palaeoclimatology, Palaeoecology 56, 337–379.
Aharon, P., Chappell, J., Compston, W., 1980. Stable isotope and sea-level data from New Guinea supports Antarctic ice-surge theory of ice ages. Nature 283, 649–651.
Alibert, C., McCulloch, M.T., 1997. Strontium/calcium ratios in modern *Porites* corals from the Great Barrier Reef as a proxy for sea surface temperature: calibration of the thermometer and monitoring of ENSO. Paleoceanography 12, 345–363.
An, Z., Wu, X., Wang, P., Wang, S., Dong, G., Sun, X., Zhang, D., Lu, Y., Zheng, S., Zhao, S., 1991. Paleomonsoons of China over the last 130,000 years-paleomonsoon variation. Science in China. Series B 34, 1016–1024.
Andreasson, F.P., Schmitz, B., 1996. Winter and summer temperatures of the early middle Eocene of France from Turritella δ18O profiles. Geology 24, 1067–1070.

Andreasson, F.P., Schmitz, B., 2000. Temperature seasonality in the early middle Eocene North Atlantic region: evidence from stable isotope profiles of marine gastropod shells. Geological Society of America Bulletin 112, 628–640.
Aubert, A., Lazareth, C., Cabioch, G., Boucher, H., Yamada, T., Iryu, Y., Farman, R., 2009. The tropical giant clam Hippopus hippopus shell, a new archive of environmental conditions as revealed by sclerochronological and $\delta^{18}O$ profiles. Coral Reefs 28, 989–998.
Batenburg, S.J., Reichart, G.J., Jilbert, T., Janse, M., Wesselingh, F.P., Renema, W., 2011. Interannual climate variability in the Miocene: high resolution trace element and stable isotope ratios in giant clams. Palaeogeography, Palaeoclimatology, Palaeoecology 306, 75–81.
Beck, J., Edwards, R., Ito, E., Taylor, F., Recy, J., Rougerie, F., Joannot, P., Henin, C., 1992. Sea-surface temperature from coral skeletal strontium/calcium ratios. Science 257, 644–647.
Bojar, A.-V., Hiden, H., Fenninger, A., Neubauer, F., 2004. Middle Miocene seasonal temperature changes in the Styrian basin, Austria, as recorded by the isotopic composition of pectinid and brachiopod shells. Palaeogeography, Palaeoclimatology, Palaeoecology 203, 95–105.
Cole, J., Fairbanks, R., Shen, G., 1993. Recent variability in the Southern Oscillation: isotopic results from a Tarawa Atoll coral. Science 260, 1790–1793.
Correge, T., 2006. Sea surface temperature and salinity reconstruction from coral geochemical tracers. Palaeogeography, Palaeoclimatology, Palaeoecology 232, 408–428.
Elliot, M., Welsh, K., Chilcott, C., McCulloch, M., Chappell, J., Ayling, B., 2009. Profiles of trace elements and stable isotopes derived from giant long-lived *Tridacna gigas* bivalves: potential applications in paleoclimate studies. Palaeogeography, Palaeoclimatology, Palaeoecology 280, 132–142.
Gagan, M., Chivas, A., Isdale, P., 1994. High-resolution isotopic records from corals using ocean temperature and mass-spawning chronometers. Earth and Planetary Science Letters 121, 549–558.
Goewert, A.E., Surge, D., 2008. Seasonality and growth patterns using isotope sclerochronology in shells of the Pliocene scallop Chesapecten madisonius. Geo-Marine Letters 28, 327–338.
Hughen, K.A., Baillie, M.G.L., Bard, E., Beck, J.W., Bertrand, C.J.H., Blackwell, P.G., Buck, C.E., Burr, G.S., Cutler, K.B., Damon, P.E., 2004. Marine04 marine radiocarbon age calibration, 0-26 cal kyr BP. Radiocarbon 46, 1059–1086.
Jones, D.S., Allmon, W.D., 1995. Records of upwelling, seasonality and growth in stable-isotope profiles of Pliocene mollusk shells from Florida. Lethaia 28, 61–74.
Maier, E., Titschack, J., 2010. Spondylus gaederopus: a new Mediterranean climate archive—based on high-resolution oxygen and carbon isotope analyses. Palaeogeography, Palaeoclimatology, Palaeoecology 291, 228–238.
McCulloch, M., Gagan, M., Mortimer, G., Chivas, A., Isdale, P., 1994. A high-resolution Sr/Ca and $\delta^{18}O$ coral record from the Great Barrier Reef, Australia, and the 1982-1983 El Nino. Geochimica et Cosmochimica Acta 58, 2747–2754.
McCulloch, M., Mortimer, G., Esat, T., Xianhua, L., Pillans, B., Chappell, J., 1996. High resolution windows into early Holocene climate: Sr/Ca coral records from the Huon Peninsula. Earth and Planetary Science Letters 138, 169–178.
Meeker, L.D., Mayewski, P.A., 2002. A 1400-year high-resolution record of atmospheric circulation over the North Atlantic and Asia. The Holocene 12, 257–266.
Oppo, D.W., Rosenthal, Y., Linsley, B.K., 2009. 2,000-year-long temperature and hydrology reconstructions from the Indo-Pacific warm pool. Nature 460, 1113–1116.
Patterson, W.P., Dietrich, K.A., Holmden, C., Andrews, J.T., 2010. Two millennia of North Atlantic seasonality and implications for Norse colonies. Proceedings of the National Academy of Sciences 107, 5306–5310.
Rosewater, J., 1965. The family *Tridacnidae* in the Indo-Pacific. Indo-Pacific Mollusca 1, 347–396.
Sano, Y., Kobayashi, S., Shirai, K., Takahata, N., Matsumoto, K., Watanabe, T., Sowa, K., Iwai, K., 2012. Past daily light cycle recorded in the strontium/calcium ratios of giant clam shells. Nature Communications 3, 761.
Schöne, B.R., Fiebig, J., 2009. Seasonality in the North Sea during the Aller d and Late Medieval Climate Optimum using bivalve sclerochronology. International Journal of Earth Sciences 98, 83–98.
Schöne, B.R., Dunca, E., Mutvei, H., Norlund, U., 2004a. A 217-year record of summer air temperature reconstructed from freshwater pearl mussels (*M-margarifitera*, Sweden). Quaternary Science Reviews 23, 1803–1816.
Schöne, B.R., Freyre Castro, A.D., Fiebig, J., Houk, S.D., Oschmann, W., Kroncke, I., 2004b. Sea surface water temperatures over the period 1884-1983 reconstructed from oxygen isotope ratios of a bivalve mollusk shell (Arctica islandica, southern North Sea). Palaeogeography, Palaeoclimatology, Palaeoecology 212, 215–232.
Schöne, B.R., Fiebig, J., Pfeiffer, M., Gless, R., Hickson, J., Johnson, A.L.A., Dreyer, W., Oschmann, W., 2005a. Climate records from a bivalved Methuselah (*Arctica islandica*, Mollusca; Iceland). Palaeogeography, Palaeoclimatology, Palaeoecology 228, 130–148.
Schöne, B.R., Pfeiffer, M., Pohlmann, T., Siegismund, F., 2005b. A seasonally resolved bottom-water temperature record for the period AD 1866–2002 based on shells of Arctica islandica (Mollusca, North Sea). International Journal of Climatology 25, 947–962.
Schrag, D.P., 1999. Rapid analysis of high-precision Sr/Ca ratios in corals and other marine carbonates. Paleoceanography 14, 97–102.
Smetacek, V., Nicol, S., 2005. Polar ocean ecosystems in a changing world. Nature 437, 362–368.
Surge, D., Barrett, J.H., 2012. Marine climatic seasonality during medieval times (10th to 12th centuries) based on isotopic records in Viking Age shells from Orkney, Scotland. Palaeogeography, Palaeoclimatology, Palaeoecology 350, 236–246.
Wanamaker, A.D., Kreutz, K.J., Schöne, B.R., Pettigrew, N., Borns, H.W., Introne, D.S., Belknap, D., Maasch, K.A., Feindel, S., 2008. Coupled North Atlantic slope water forcing on Gulf of Maine temperatures over the past millennium. Climate Dynamics 31, 183–194.
Wanamaker, A.D., Kreutz, K.J., Schöne, B.R., Introne, D.S., 2011. Gulf of Maine shells reveal changes in seawater temperature seasonality during the Medieval Climate Anomaly and the Little Ice Age. Palaeogeography, Palaeoclimatology, Palaeoecology 302, 43–51.
Wang, T., Surge, D., Mithen, S., 2012. Seasonal temperature variability of the Neoglacial (3300–2500BP) and Roman Warm Period (2500–1600BP) reconstructed from oxygen isotope ratios of limpet shells (*Patella vulgata*), Northwest Scotland. Palaeogeography, Palaeoclimatology, Palaeoecology 317, 104–113.
Wang, T., Surge, D., Walker, K.J., 2013. Seasonal climate change across the Roman Warm Period/Vandal Minimum transition using isotope sclerochronology in archaeological shells and otoliths, southwest Florida, USA. Quaternary International 308, 230–241.
Watanabe, T., Oba, T., 1999. Daily reconstruction of water temperature from oxygen isotopic ratios of a modern *Tridacna* shell using a freezing microtome sampling technique. Journal of Geophysical Research-Oceans 104, 20667–20674.
Watanabe, T., Suzuki, A., Kawahata, H., Kan, H., Ogawa, S., 2004. A 60-year isotopic record from a mid-Holocene fossil giant clam (*Tridacna gigas*) in the Ryukyu Islands: physiological and paleoclimatic implications. Palaeogeography, Palaeoclimatology, Palaeoecology 212, 343–354.
Wei, G.J., Sun, M., Li, X.H., Nie, B.F., 2000. Mg/Ca, Sr/Ca and U/Ca ratios of a *Porites* coral from Sanya Bay, Hainan Island, South China Sea and their relationships to sea surface temperature. Palaeogeography, Palaeoclimatology, Palaeoecology 162, 59–74.
Wei, G.J., Deng, W.F., Yu, K.F., Li, X.H., Sun, W.D., Zhao, J.X., 2007. Sea surface temperature records in the northern South China Sea from mid-Holocene coral Sr/Ca ratios. Paleoceanography 22, PA3206.
Weninger, B., Jöris, O., Danzeglocke, U., 2007. CalPal-2007. Cologne Radiocarbon Calibration & Palaeoclimate Research Package. Radiocarbon Laboratory, Cologne University, Cologne, Germany.
Yan, H., Sun, L., Liu, X., Qiu, S., 2010a. Relationship between ENSO events and regional climate anomalies around the Xisha Islands during the last 50 years. Journal of Tropical Oceanography 29, 29–35 (In Chinese with English abstract).
Yan, H., Sun, L.G., Wang, Y.H., Liu, X.D., Qiu, S.C., Cheng, W.H., 2010b. A 2000-year record of copper pollution in South China Sea derived from seabird excrements: a potential indicator for copper production and civilization of China. Journal of Paleolimnology 44, 431–442.
Yan, H., Shao, D., Wang, Y.-h., Sun, L.-g., 2011a. High resolution Sr/Ca profile of *Tridacna gigas* from Xisha Islands of South China Sea and its potential application on sea surface temperature reconstruction. Journal of Earth Environment 381–386 (In Chinese with English abstract).
Yan, H., Sun, L., Oppo, D.W., Wang, Y., Liu, Z., Xie, Z., Liu, X., Cheng, W., 2011b. South China Sea hydrological changes and Pacific Walker Circulation variations over the last millennium. Nature Communications 2, 293.
Yan, H., Shao, D., Wang, Y., Sun, L., 2013. Sr/Ca profile of long-lived *Tridacna gigas* bivalves from South China Sea: a new high-resolution SST proxy. Geochimica et Cosmochimica Acta 112, 52–65.
Yan, H., Shao, D., Wang, Y., Sun, L., 2014a. Sr/Ca differences within and among three Tridacna species from the South China Sea: implication for paleoclimate reconstruction. Chemical Geology 390, 22–31.
Yan, H., Sun, L., Shao, D., Wang, Y., 2014b. Higher Sea surface temperature in the northern South China Sea during the natural warm periods of late Holocene than recent decades. Chinese Science Bulletin 59, 4115–4122.
Yan, H., Wang, Y., Sun, L., 2014c. High resolution oxygen isotope and grayscale records of a medieval fossil giant clam (*Tridacna gigas*) in the South China Sea: physiological and paleoclimatic implications. Acta Oceanologica Sinica 33, 18–25.
Yu, K., Zhao, J., Wei, G., Cheng, X., Wang, P., 2005a. Mid-late Holocene monsoon climate retrieved from seasonal Sr/Ca and $\delta^{18}O$ records of *Porites lutea* corals at Leizhou Peninsula, northern coast of South China Sea. Global and Planetary Change 47, 301–316.
Yu, K.F., Zhao, J.X., Wei, G.J., Cheng, X.R., Chen, T.G., Felis, T., Wang, P.X., Liu, T.S., 2005b. delta O-18, Sr/Ca and Mg/Ca records of *Porites lutea* corals from Leizhou Peninsula, northern South China Sea, and their applicability as paleoclimatic indicators. Palaeogeography, Palaeoclimatology, Palaeoecology 218, 57–73.

https://doi.org/10.1016/j.yqres.2014.12.001 Published online by Cambridge University Press